ELSEVIER

Applied Ocean Research 22 (2000) 295–314

Applied Ocean Research

www.elsevier.com/locate/apor

Green functions for hydroelastic analysis of vibrating free–free beams and plates

R. Eatock Taylor[a,*], M. Ohkusu[b]

[a]*Department of Engineering Science, University of Oxford, Parks Road, Oxford OX1 3PJ, UK*
[b]*Research Institute for Applied Mechanics, Kyushu University, 6-1 Kasuga-koen, Kasuga City, Fukuoka 816, Japan*

Abstract

Closed form expressions for the Green function of flexural vibrations of uniform beams are well known, giving the response at any point in the beam due to harmonic point excitation at any position along the beam. The expressions involve trigonometric and hyperbolic functions. The present work first develops alternative forms for the free–free beam, in terms of the sinusoidal eigenmodes of a pinned–pinned beam plus the rigid body modes. Convergence is assessed by comparison with the well-known classical results for a free–free beam. The analysis is then extended to the case of free–free rectangular plates of arbitrary aspect ratio. The work is motivated by the desirability of employing sinusoidal modes for the structure when undertaking hydroelastic analysis (e.g. for a flexible beam or plate floating in the sea).

Keywords: Green functions; Hydroelastic analysis; Free–free beams and plates

1. Introduction

There is great current interest in developing design procedures for floating islands. These would be very large structures that would be inherently rather flexible: the prime example of this is the floating plate. Analysis of the wave-induced dynamics of such a plate brings together the study of hydrodynamics and structural mechanics, in the discipline of hydroelasticity. This paper is motivated by the need to extend the classical results from vibration theory into a framework that can conveniently encompass the hydrodynamic analysis.

Detailed design of such structures will inevitably require complex numerical analysis, and progress is being made in developing appropriate hydrodynamic representations which could be coupled with finite element models of the structure. Because of the large horizontal dimensions of, say, a floating airport, conventional panel methods may be an unwieldy way of treating the hydrodynamics, and various alternatives are under development (e.g. Utsunomiya et al. [1], Kashiwagi [2], Ohkusu and Namba [3], Kagemoto et al. [4], and several others in the Proceedings of the International Workshop on Very Large Floating Structures, Hayama, Japan, 1996).

For concept design and developing an understanding of the hydroelastic phenomena, it is more convenient to adopt classical methods of analysis where possible. Short wavelength assumptions, for example, may be invoked to simplify the hydrodynamics (e.g. Ohkusu and Namba [5], Hermans [6]). The structural model may be simplified by considering the case of a homogeneous rectangular plate of uniform thickness. The vibration behaviour may be characterised by that of such a plate with free–free boundary conditions. The mode shapes can then in principle be used directly in the coupled hydroelastic analysis by solving the hydrodynamic radiation problems corresponding to the various modal displacements; or by forming the Green function corresponding to the structural response to a harmonically oscillating point load on the plate. The latter approach is adopted here, as explained in Section 2.

Whereas for a beam the free–free modes are well known and simple to write down, no such simple forms are known for a free–free plate. One approach used in some of the above-mentioned investigations is to use a sum of products of the free–free beam modes (associated with behaviour in the directions of the orthogonal axes of the rectangular plate). Although each term in the series does not satisfy the full set of boundary conditions for the free–free plate, the idea is to use sufficient terms in the series that a satisfactory representation of the plate dynamics is obtained in the limit. This may be the case when an energy formulation is used (e.g. to satisfy the natural boundary conditions

* Corresponding author. Tel.: +44-1865-273002; fax: +44-1865-273010.

E-mail address: r.eatocktaylor@eng.ox.ac.uk (R Eatock Taylor).

0141-1187/00/$ - see front matter
PII: S0141-1187(00)00018-3

implicitly), but not generally. Herein lies the motivation for this paper. Furthermore, the free–free beam modes are not in fact convenient to use when large numbers of modes need to be included, and satisfactory convergence is difficult to achieve.

Our approach, instead, is to use sinusoidal modes in combination with the rigid body modes of the plate. This has the advantage of very easy computation, and the possible benefits that may ensue from combining a Fourier representation of the structural Green function with an appropriate hydrodynamic analysis. To lay out the basis of the approach, we first examine in detail the implications of expressing the free–free beam modes themselves as a sum of sinusoids plus the rigid body modes. In Section 3, we briefly recapitulate the classical analysis of the Green function for the beam. Next, in Section 4, we develop series forms involving summations of sinusoids plus the two rigid body modes of the beam, using two different approaches. The first is a direct formulation, applying the Stokes transformation (Chen et al. [7]). This clarifies how the boundary conditions specifying zero shear at each end can be satisfied when the third derivative of each sinusoidal term in the summation for the deflected shape of the beam is itself non-zero. (In effect, the Stokes transformation deals with the Gibbs phenomenon in the Fourier series expression for the shear). The second method outlined in Section 4 is the use of an energy approach to obtain the Green function for the beam. This paves the way for using a similar approach, in Section 7, for the free–free plate. Numerical results are given to demonstrate convergence: results for the beam are provided in Section 6, and for the plate in Section 8.

2. The plate Green function in the hydroelastic context

The motivation for focussing here on the plate Green function may be illustrated by summarising how it arises in the hydroelastic analysis. Suppose we are concerned with the linear response of a flexible plate to incident waves of frequency ω. It is convenient to introduce a time harmonic velocity potential ϕ corresponding to the resulting flow, and the associated incident wave potential ϕ_I. The thin plate of area A is supposed to lie in the plane $z = 0$, where we are using a coordinate system located in the mean free surface with z positive upwards.

We first introduce the usual fluid Green function $G(\mathbf{x}; \mathbf{x}')$ corresponding to a time harmonic unit wave source. It is then easy to show that the total potential ϕ satisfies the following integral equation:

$$\phi + \int\int_A \phi \frac{\partial G_f}{\partial z}\, dA = \int\int_A G_f \frac{\partial \phi}{\partial z}\, dA + \phi_I. \tag{1}$$

ϕ, however, and in particular $\partial\phi/\partial z$ in the second integral, depends on the transverse displacement of the plate, denoted w. Furthermore, the plate is excited by the dynamic pressure, p.

Without dwelling at this stage on the specific elastic characteristics of the plate, we may state that its equation of motion is of the general form

$$Lw = p, \tag{2}$$

where the operator L involves the elastic and inertial properties. This provides the dynamic boundary condition over A for the boundary value problem satisfied by ϕ.

The kinematic boundary condition linking the plate and fluid over the interface A is

$$\frac{\partial \phi}{\partial z} = i\omega w \tag{3}$$

(where the time variation is assumed to be proportional to $\exp i\omega t$).

The dynamic pressure may be written in terms of the velocity potential as

$$p = -i\omega\rho\phi \tag{4}$$

where ρ is the density of the fluid. Hence we would have all the ingredients required to solve Eq. (1) directly for ϕ, if we could reformulate Eq. (2) to express w directly in terms of p (or ϕ).

This last step is achieved through use of the plate Green function $g_p(x, x'; y, y')$. By appropriately defining the parameters (as described below), we can write the solution of Eq. (2) as

$$w = \int\int_A p g_p\, dA. \tag{5}$$

Finally, by making the substitutions in Eq. (1), we obtain the required integral equation for the potential:

$$\phi + \omega^2 \int\int_A \left[\frac{1}{g}\phi - \rho \int\int_A \phi g_p\, dA'\right] G_f\, dA = \phi_I, \tag{6}$$

where we have also used the condition satisfied by the fluid Green function on $z = 0$, namely

$$\frac{\partial G_f}{\partial z} - \frac{\omega^2}{g} G_f = 0. \tag{7}$$

Once Eq. (6) is solved, it is straightforward to obtain w, the transverse displacement of the plate, by substituting the solution into Eq. (4) and then Eq. (5). One of the present authors has numerically solved the two-dimensional version of Eq. (6) to obtain w for a long plate in oblique waves [5]. The results for w computed up to the frequency given by $\omega^2/gB = 40\pi$ (B being the plate width) were computed using a plate Green function given as products of hyberbolic functions [8].

The key to the analysis is seen to lie in having an effective means to evaluate the coupling integral

$$I = \int\int_A \int\int_A \phi g_p G_f\, dA'\, dA. \tag{8}$$

It is this which has motivated the development below of a simple functional form for the plate Green function g_p.

It is well known that such a Green function can in principle be expressed in terms of the modes of vibration of the plate. Previous investigations have sought to approximate the modes and corresponding frequencies of a free–free plate. Leissa [9] used the known free–free beam modes, based on the approach mentioned in the previous section. Bardell [10] used products of Legendre polynomials in the x and y directions, coupled with the cubic shape functions for beam finite elements, to approximate the natural frequencies of plates with a variety of edge conditions, including all edges free. Beslin and Nicolas [11] pointed out that the polynomial approach was badly conditioned numerically, if one were seeking natural frequencies corresponding to very high modes, or highly converged results. These authors developed an alternative approach based on trigonometric functions, and showed that over 2000 terms in the series could be used in each direction without any numerical problems. Each term in each direction, however, involves a product of two trigonometric terms.

The method described below uses products of single trigonometric terms, which seems to be more convenient for developing the plate Green function (which does not appear to have been tackled by the afore-mentioned authors). Furthermore, such simple series would seem to be very appropriate for use in the complex integral I defined above.

3. The closed form expression for the free–free beam

By way of introduction to our approach, we first investigate the simpler case of the free–free beam. We consider a uniform beam of length L, mass per unit length m and flexural rigidity EI. The analysis is based on Euler–Bernoulli beam theory, so that effects of shear deformations and rotary inertia are ignored. The transverse deflection of the beam is $v(x, t)$, where t is time and the coordinate x is measured from the left-hand end of the beam. Under a load per unit length $f(x, t)$, the deflection of the beam satisfies the equation.

$$EI\frac{\partial^4 v}{\partial x^4} + m\frac{\partial^2 v}{\partial t^2} = f. \tag{9}$$

We define the Green function, $g(x; x')$, as the deflection at x corresponding to a point load $\delta(x - x')$ of unit amplitude at frequency ω at position x', $\delta(x)$ being the Dirac delta function. Thus $g(x; x')$ satisfies

$$\frac{\mathrm{d}^4 g}{\mathrm{d}x^4} - \beta^4 g = \frac{1}{EI}\delta(x - x') \tag{10}$$

where $\beta^4 = m\omega^2/EI$. Applying the boundary conditions of zero moment and shear at each end of the free–free beam we have

$$\frac{\mathrm{d}^2 g}{\mathrm{d}x^2} = 0 \qquad \text{at } x = 0, L; \tag{11}$$

$$\frac{\mathrm{d}^3 g}{\mathrm{d}x^3} = 0 \qquad \text{at } x = 0, L. \tag{12}$$

Milne [12] has given a general formulation for all possible boundary conditions of a uniform beam, from which we may extract the solution corresponding to free–free end conditions as follows:

$$\begin{aligned} 4EI\beta^3(1 - \cosh\beta L\cos\beta L)g(x; x') &= (\cosh\beta L - \cos\beta L)[E_1(x)E_2(L - x') + E_2(x)E_1(L - x')] \\ &\quad - \sinh\beta L[E_1(x)E_1(L - x') + E_2(x)E_2(L - x')] \\ &\quad - \sin\beta L[E_1(x)E_1(L - x') - E_2(x)E_2(L - x')], \\ 0 \le x \le x'; \end{aligned} \tag{13}$$

where

$$E_1(x) = \sinh\beta x + \sin\beta x,$$

$$E_2(x) = \cosh\beta x + \cos\beta x.$$

The solution for $x' \le x \le L$ is obtained by exchanging x and $(L - x')$ in the various terms of Eq. (13). It is apparent that at high frequencies (large values of β) these expressions are badly conditioned, and they may be written in an alternative form by first extracting the term $\exp(\beta L)$. This procedure for improving the accuracy of calculation at high frequency has been described by Beshara [13].

4. Alternative forms of Green function for the beam

4.1. Direct derivation of an appropriate series form

We start by considering the solution to Eq. (9) in the form

$$v(x, t) = \sum_{n=1}^{\infty} P_n(t)\psi_n(x) + v_1(t)\left(1 - \frac{x}{L}\right) + v_2(t)\left(\frac{x}{L}\right), \tag{14}$$

$0 \le x \le L.$

We use the modes of a simply supported beam, taken as

$$\psi_n(x) = \sin\left(\frac{n\pi x}{L}\right);$$

and deffine $v_1(t)$ and v_2(t) as the deflections at the left and right-hand ends, respectively, of the free–free beam. While Eq. (14) satisfies the conditions of zero moment at each end of the free–free beam, it is clear that a non-trivial solution satisfying the conditions of zero shear is not achieved by direct differentiation of this equation, term-by-term. To overcome this problem, associated with the Gibbs phenomenon in Fourier series, we may use the Stokes transformation for differentiation of the series. The approach has been described by Chen et al. [7] in the context of structural

dynamics. The starting point is to write

$$v(x,t) = \sum_{n=1}^{\infty} P_n(t)\psi_n(x), \qquad 0 < x < L \tag{15}$$

with $\psi_n(x)$ as defined above, and the corresponding relation

$$P_n(t) = \frac{2}{L}\sum_{0}^{L} v(x,t)\psi_n(x)\,\mathrm{d}x. \tag{16}$$

The series differentiation by Stokes transformation leads to

$$v'(x,t) = \sum_{n=1}^{\infty} P'_n(t)\psi'_n(x) \tag{17}$$

where the prime on the functions of x designates differentiation with respect to x, and we define (following Chen et al. [7])

$$P'_n(t) = \frac{2}{L}\left(\frac{L}{n\pi}\right)^2 \int_0^L v'(x,t)\psi'_n(x)\,\mathrm{d}x$$

$$= \frac{2}{L}\left(\frac{L}{n\pi}\right)^2 [v(x,t)\psi'_n(x)]_0^L + P_n(t). \tag{18}$$

To obtain the last expression, we have used Eq. (16) and the result

$$\psi''_n = -\left(\frac{n\pi}{L}\right)^2 \psi_n. \tag{19}$$

Inserting the values at $x = 0$, L and the definition of $\psi_n(x)$, we thus obtain

$$P'_n(t) = -\frac{2}{n\pi}[v_1 + (-1)^{n+1}v_2] + P_n(t). \tag{20}$$

We continue to differentiate the series in this manner, obtaining the following:

$$v''(x,t) = \sum_{n=1}^{\infty} P''_n(t)\psi''_n(x) \tag{21}$$

with

$$P''_n(t) = \left(\frac{2}{L}\right)\left(\frac{L}{n\pi}\right)^4 [v'(x,t)\psi''_n(x)]_0^L + P'_n(t) = P'_n(t); \tag{22}$$

$$v'''(x,t) = \sum_{n=1}^{\infty} P'''_n(t)\psi'''(x) \tag{23}$$

with

$$P'''_n(t) = \left(\frac{2}{L}\right)\left(\frac{L}{n\pi}\right)^6 [v''(x,t)\psi'''_n(x)]_0^L + P''_n(t) = P'_n(t); \tag{24}$$

and

$$v''''(x,t) = \sum_{n=1}^{\infty} P''''_n(t)\psi''''_n(x) \tag{25}$$

with

$$P''''_n(t) = \left(\frac{2}{L}\right)\left(\frac{L}{n\pi}\right)^8 [v'''(x,t)\psi''''_n(x)]_0^L + P'''_n(t) = P'_n(t). \tag{26}$$

In obtaining Eq. (24) we have used the zero moment boundary condition on $v(x, t)$.

Next we integrate Eq. (25) four times with respect to x, using the zero moment boundary conditions to eliminate the two arbitrary constants thereby introduced. We impose the zero shear conditions subsequently. This leads to:

$$v(x,t) = v_1(t)\left(1 - \frac{x}{L}\right) + v_2(t)\left(\frac{x}{L}\right) + \sum_{n=1}^{\infty} P'_n(t)\psi_n(x)$$

$$= v_1(t)\left[\left(1 - \frac{x}{L}\right) - \sum_{n=1}^{\infty}\frac{2}{n\pi}\sin\left(\frac{n\pi x}{L}\right)\right] + v_2(t)$$

$$\times\left[\left(\frac{x}{L}\right) - \sum_{n=1}^{\infty}(-1)^{n+1}\frac{2}{n\pi}\sin\left(\frac{n\pi x}{L}\right)\right]$$

$$+ \sum_{n=1}^{\infty} P_n(t)\sin\frac{n\pi x}{L}. \tag{27}$$

The summations in the square brackets are of course simply the Fourier series for the two rigid body modes, given by the first term in each set of square brackets. Hence, the contents of these brackets are zero for $0 < x < L$, but for any finite number of terms in the series they have the desired property of being non-zero at the ends. By this means, we are able to satisfy the zero shear boundary conditions when we use the series of modes for a simply supported beam.

4.2. Solution for the coefficients in the series

We obtain v_1, v_2 and P_n corresponding to the Green function by first substituting Eq. (27) into the equation of motion (10), and by taking

$$v(x,t) = g(x;x')\cos\omega t; \qquad P_n(t) = \bar{P}_n\cos\omega t, \text{ etc.}$$

It is convenient, however, to omit the overbar in the following.

We multiply the resulting equation by $\psi_m(x)$, and integrate over the length of the beam. This yields

$$\frac{n^4\pi^4}{L^4}\left[P_n - (v_1 + (-1)^{n+1}v_2)\frac{2}{n\pi}\right] - \beta^4 P_n$$

$$= \frac{2}{EIL}\sin\left(\frac{n\pi x'}{L}\right), \tag{28}$$

noting that the terms in the square brackets of Eq. (27) do not contribute to the distributed inertia term (the v_1 and v_2 parts do, however, contribute to the stiffness term, since at this stage we can use term-by-term differentiation). Hence,

we obtain

$$P_n = \frac{1}{n^4 - \mu^4}\left[\frac{2}{\pi} n^3 [v_1 + (-1)^{n+1} v_2] + \frac{2}{\pi} \frac{L^3}{\pi^3 EI} \sin\left(\frac{n\pi x'}{L}\right)\right] \tag{29}$$

where we define μ through

$$\beta^4 = \frac{m\omega^2}{EI} = \frac{\mu^4 \pi^4}{L^4}. \tag{30}$$

Next we substitute Eq. (29) into Eq. (27), leading to

$$\begin{aligned} g(x;x') = {} & v_1 \left\{ \left(1 - \frac{x}{L}\right) + \sum_{n=1}^{\infty} \frac{2}{n\pi} \sin\left(\frac{n\pi x}{L}\right) \times \left[-1 + \frac{n^4}{n^4 - \mu^4} \right] \right\} \\ & + v_2 \left\{ \left(\frac{x}{L}\right) + \sum_{n=1}^{\infty} \frac{2}{n\pi} (-1)^{n+1} \sin\left(\frac{n\pi x}{L}\right) \times \left[-1 + \frac{n^4}{n^4 - \mu^4} \right] \right\} \\ & + \frac{2L^3}{\pi^4 EI} \sum_{n=1}^{\infty} \frac{1}{n^4 - \mu^4} \sin\left(\frac{n\pi x}{L}\right) \sin\left(\frac{n\pi x'}{L}\right). \end{aligned} \tag{31}$$

From the zero shear boundary condition at $x = 0$ we obtain

$$\sum_{n=1}^{\infty} \left\{ \frac{n^2 \mu^4}{n^4 - \mu^4} [v_1 + (-1)^{n+1} v_2] + \frac{n^3}{n^4 - \mu^4} \frac{L^3}{\pi^3 EI} \sin\left(\frac{n\pi x'}{L}\right) \right\} = 0 \tag{32}$$

and the corresponding condition at $x = L$ yields

$$\sum_{n=1}^{\infty} (-1)^{n+1} \left\{ \frac{n^2 \mu^4}{n^4 - \mu^4} [v_1 + (-1)^{n+1} v_2] + \frac{n^3}{n^4 - \mu^4} \frac{L^3}{\pi^3 EI} \sin\left(\frac{n\pi x'}{L}\right) \right\} = 0. \tag{33}$$

These two equations are to be solved for v_1 and v_2, and it is convenient to introduce the following definitions:

$$A_1 = \frac{2}{\pi} \sum_{n=1}^{\infty} \frac{n^2 \mu^4}{n^4 - \mu^4}; \qquad A_2 = \frac{2}{\pi} \sum_{n=1}^{\infty} (-1)^{n+1} \frac{n^2 \mu^4}{n^4 - \mu^4}; \tag{34}$$

$$\begin{aligned} Q_1(x') &= \frac{2}{\pi} \sum_{n=1}^{\infty} \frac{n^3}{n^4 - \mu^4} \sin\left(\frac{n\pi x'}{L}\right); \\ Q_2(x') &= \frac{2}{\pi} \sum_{n=1}^{\infty} (-1)^{n+1} \frac{n^3}{n^4 - \mu^4} \sin\left(\frac{n\pi x'}{L}\right). \end{aligned} \tag{35}$$

All of these series may be summed up in closed form. We proceed as follows. Taking

$$A_1 = \sum_{n=1}^{\infty} \frac{1}{\pi} \left[\frac{\mu^4}{n^2 - \mu^2} + \frac{\mu^4}{n^2 + \mu^2} \right], \tag{36}$$

we may use a result in Bromwich ([14], p. 36):

$$1 + \sum_{n=1}^{\infty} \frac{(-1)^n 2\mu^2 \cos n\theta}{n^2 + \mu^2} = \mu\pi \frac{\cosh \mu\theta}{\sinh \mu\pi}. \tag{37}$$

Replacing θ by π in Eq. (37) we obtain

$$\sum_{n=1}^{\infty} \frac{\mu^2}{n^2 + \mu^2} = -\frac{1}{2} + \frac{\mu\pi}{2} \coth \mu\pi; \tag{38}$$

and replacing μ by $i\mu$ in Eq. (38) we obtain

$$\sum_{n=1}^{\infty} \frac{\mu^2}{n^2 - \mu^2} = \frac{1}{2} - \frac{\mu\pi}{2} \cot \mu\pi. \tag{39}$$

This leads immediately to

$$A_1 = \frac{\mu^3}{2} (\coth \mu\pi - \cot \mu\pi). \tag{40}$$

In a similar manner, replacing θ by 0 in Eq. (37), we can obtain

$$A_2 = \frac{-\mu^3}{2} (\operatorname{cosech} \mu\pi - \operatorname{cosec} \mu\pi). \tag{41}$$

It is convenient to retain the summations in Q_1 and Q_2, but in the following form. We have

$$\begin{aligned} Q_1(x') &= \frac{2}{\pi} \sum_{n=1}^{\infty} \frac{n^3}{n^4 - \mu^4} \sin\left(\frac{n\pi x'}{L}\right) \\ &= \frac{2}{\pi} \sum_{n=1}^{\infty} \frac{1}{n} \left(1 + \frac{\mu^4}{n^4 - \mu^4}\right) \sin\left(\frac{n\pi x'}{L}\right), \end{aligned} \tag{42}$$

or

$$Q_1(x') = \left(1 - \frac{x'}{L}\right) + \frac{2}{\pi} \sum_{n=1}^{\infty} \frac{\mu^4}{n(n^4 - \mu^4)} \sin\left(\frac{n\pi x'}{L}\right) \tag{43}$$

where the first sum has been closed by again using Bromwich ([14], p. 188). Similarly we find

$$Q_2(x') = \left(\frac{x'}{L}\right) + \frac{2}{\pi} \sum_{n=1}^{\infty} \frac{(-1)^{n+1} \mu^4}{n(n^4 - \mu^4)} \sin\left(\frac{n\pi x'}{L}\right). \tag{44}$$

Eqs. (32) and (33) are now written in the form

$$A_1 v_1 + A_2 v_2 = -\frac{L^3}{\pi^3 EI} Q_1(x') \tag{45}$$

$$A_2 v_1 + A_1 v_2 = -\frac{L^3}{\pi^3 EI} Q_2(x'). \tag{46}$$

The solution may be readily found as

$$v_1 = \frac{L^3}{\pi^3 EI}[\alpha_1 Q_1(x') + \alpha_2 Q_2(x')], \tag{47}$$

$$v_2 = \frac{L^3}{\pi^3 EI}[\alpha_2 Q_1(x') + \alpha_1 Q_2(x')], \tag{48}$$

where

$$\alpha_1 = -\frac{1}{\mu^3}\frac{\cos \mu\pi \sinh \mu\pi - \cosh \mu\pi \sin \mu\pi}{\cosh \mu\pi \cos \mu\pi - 1};$$
$$\alpha_2 = -\frac{1}{\mu^3}\frac{\sin \mu\pi - \sinh \mu\pi}{\cosh \mu\pi \cos \mu\pi - 1}. \tag{49}$$

These may also be written in alternative forms suited to evaluation at high frequencies. We define

$$\rho = \exp(-\mu\pi) \tag{50}$$

and express α_1, α_2 as follows:

$$\alpha_1 = -\frac{1}{\mu^3}\frac{(1-\rho^2)\cos \mu\pi - (1+\rho^2)\sin \mu\pi}{(1+\rho^2)\cos \mu\pi - 2\rho};$$
$$\alpha_2 = -\frac{1}{\mu^3}\frac{2\rho \sin \mu\pi - (1-\rho^2)}{(1+\rho^2)\cos \mu\pi - 2\rho}. \tag{51}$$

Substituting Eqs. (47) and (48) into Eq. (31), and noting the definition for Q_1 and Q_2 in Eqs. (43) and (44), we obtain:

$$g(x;x') = \frac{L^3}{\pi^3 EI}\Bigg\{[\alpha_1 Q_1(x') + \alpha_2 Q_2(x')]Q_1(x) + [\alpha_2 Q_1(x') + \alpha_1 Q_2(x')]Q_2(x) + \frac{2}{\pi}\sum_{n=1}^{\infty}\frac{1}{n^4-\mu^4}\sin\left(\frac{n\pi x}{L}\right)\sin\left(\frac{n\pi x'}{L}\right)\Bigg\}. \tag{52}$$

This is the required form of the Green function obtained by the Stokes transformation. We designate this "series form A", to distinguish it from that derived in Section 4.3. It may be noted that the expression for $g(x,x')$ is symmetric in x and x', and there is no need to distinguish between the cases $x < x'$ and $x > x'$.

It is easy to verify that this expression gives the usual tip receptances for the free–free beam. Thus,

$$g(0;0) = \frac{L^3}{\pi^3 EI}\alpha_1; \qquad g(0;L) = \frac{L^3}{\pi^3 EI}\alpha_2.$$

We also note that the series in Eq. (52), and those in the definitions of Q_1 and Q_2 (Eqs. (43) and (44)) all converge very fast. It may be anticipated that this form will have satisfactory numerical characteristics, with the possible exception of frequencies close to the natural frequencies of the simply supported beam(i.e. $\mu \to n$). This can be checked through numerical experiments, and is discussed below.

4.3. Derivation by the energy method

We now apply classical energy methods to obtain the coefficients in the series form of the deflection. Starting from Hamilton's principle, and assuming harmonic excitation and response, it is easy to derive the variational form

$$\delta(U - T + V) = 0, \tag{53}$$

where for the uniform beam

$$U = \frac{EI}{2}\int_0^L \left(\frac{\mathrm{d}^2 v}{\mathrm{d}x^2}\right)^2 \mathrm{d}x; \qquad T = \frac{m}{2}\omega^2 \int_0^L v^2\,\mathrm{d}x;$$
$$V = -\int_0^L fv\,\mathrm{d}x. \tag{54}$$

We use this for the case of the unit point load on the beam, introducing the definitions given earlier, and taking the deflection of the beam in the simple series form given in Eq. (14). Performing the integrations, we obtain

$$U = \frac{EI}{4L^3}\sum_n n^4\pi^4 P_n^2; \tag{55}$$

$$T = \frac{1}{2}\omega^2 mL\Bigg\{\frac{1}{3}(v_1^2 + v_1 v_2 + v_2^2) + \sum_n \frac{1}{2}P_n^2 + \sum_n \frac{2}{n\pi}[v_1 + v_2(-1)^{n+1}]P_n\Bigg\} \tag{56}$$

$$V = -v_1 - v_2\frac{x'}{L} - \sum_{n=1}^{\infty} P_n \sin\left(\frac{n\pi x'}{L}\right). \tag{57}$$

Taking the variation with respect to the unknown coefficients v_1, v_2 and P_n, we can write the resulting equations in the matrix form

$$(\mathbf{K} - \mu^4\mathbf{M})\mathbf{Q} = \mathbf{F} \tag{58}$$

where

$$\mathbf{Q}^{\mathrm{T}} = [v_1 \quad v_2 \quad P_1 \quad P_2 \ldots P_n \ldots]; \tag{59}$$

$$\mathbf{F} = \left[1 \quad \frac{x'}{L} \quad \sin\left(\frac{\pi x'}{L}\right) \quad \sin\left(\frac{2\pi x'}{L}\right)\ldots \sin\left(\frac{n\pi x'}{L}\right)\ldots\right]; \tag{60}$$

$$\mathbf{K} = \begin{bmatrix}\mathbf{O} & \mathbf{O}\\ \mathbf{O} & \mathbf{K}_{PP}\end{bmatrix}; \qquad \mathbf{M} = \begin{bmatrix}\mathbf{M}_{vv} & \mathbf{M}_{vP}\\ \mathbf{M}_{Pv} & \mathbf{M}_{PP}\end{bmatrix}. \tag{61}$$

The non-zero terms of the symmetric submatrices are obtained from:

$$M_{v1v1} = \tfrac{2}{3};$$

$$M_{v1v2} = \tfrac{1}{3};$$

$$M_{v2v2} = \tfrac{2}{3};$$

$$M_{v1Pn} = \sum_n \frac{2}{n\pi};$$

$$M_{v2Pn} = \sum_n \frac{2}{n\pi}(-1)^{n+1};$$

$$M_{PnPn} = 1;$$

$$K_{PnPn} = n^4.$$

For the beam it is possible to solve this infinite set of equations exactly, by noting that the variation with respect to P_n yields

$$P_n = \frac{\mu^4}{n^4 - \mu^4}\left[\frac{2}{n\pi}(v_1 + (-1)^{n+1}v_2) + \frac{2}{mL\omega^2}\sin\left(\frac{n\pi x'}{l}\right)\right]. \tag{62}$$

Substitution of this into the other two equations, and summation of the infinite series using the definitions for A_1 and A_2 in Eq. (34) and Q_1 and Q_2 in Eqs. (43) and (44), leads directly to Eqs. (45) and (46). It is important to note, however, that in the energy approach we have started from the deflected shape given by Eq. (14), whereas in arriving before at Eqs. (45) and (46), we used the extended form of $v(x,t)$ given in Eq. (27). This is because the natural boundary conditions on shear are satisfied implicitly by the energy formulation.

It is of course also possible, and convenient, to solve for Q by direct inversion of the matrix Eq. (58), truncated at a finite number of terms in the series, and hence to obtain an approximation to the Green function. We identify this approach as "series form B".

In Section 6, we compare numerical results from the two series formulations of the Green function with the exact solution. First, however, we summarise the step from the Green function to the response to a distributed load.

5. Application to a beam with a distributed load

One of the aims of this analysis is to have the Green function in a form which can simply be used in a hydroelastic analysis, where the fluid problem is represented by some distribution of load on the flexible structure. Rather than solve the complete coupled problem here, we illustrate the convenience of the present approach when the hydrodynamic load has been expressed as a Fourier series. A characteristic example is that of a free–free plate or beam subject to a distributed load which decreases monotonically from one end (say the left-hand end $x = 0$ for the beam). This is related to the envelope of the wave force associated with diffraction of free surface waves encountering a floating beam.

To fix ideas, we assume a parabolic load distribution of the form

$$f(x) = \begin{cases} \dfrac{3}{2c^3}(c^2 - x^2), & 0 < x \le c \\ 0, & c < x < L \end{cases} \tag{63}$$

Thus, the force per unit length reduces to zero at $x = $ c, and the total load is always unity for any value of c. It is easy to show that this may be expressed as the Fourier series

$$f(x) = \sum_{n=1}^{\infty} F_n \sin\left(\frac{n\pi x}{L}\right), \tag{64}$$

where

$$F_n = \frac{3}{L}\left[\frac{1}{\gamma_n} - \frac{2}{\gamma_n^2}\sin\gamma_n + \frac{2}{\gamma_n^3}(1 - \cos\gamma_n)\right] \tag{65}$$

and

$$\gamma_n = \frac{n\pi c}{L}. \tag{66}$$

The response of the beam to the distributed load, varying with time at frequency ω, is written in terms of the Green function as

$$v_d(x) = \int_0^L g(x,x')f(x')\,dx' \tag{67}$$

where $g(x;x')$ is given by Eq. (52). Noting that

$$\int_0^L \left(1 - \frac{x'}{L}\right)f(x')\,dx' = 1 - \frac{3}{8}\frac{c}{L},$$

$$\int_0^L \left(\frac{x'}{L}\right)f(x')\,dx' = \frac{3}{8}\frac{c}{L},$$

we readily obtain

$$v_d(x) = \frac{L^3}{\pi^3 EI}\left[(\alpha_1 V_1 + \alpha_2 V_2)Q_1(x) + (\alpha_2 V_1 + \alpha_1 V_2)Q_2(x) + \frac{L}{\pi}\sum_{n=1}^{\infty}\frac{F_n}{n^4 - \mu^4}\sin\left(\frac{n\pi x}{L}\right)\right] \tag{68}$$

where

$$V_1 = \left(1 - \frac{3}{8}\frac{c}{L} + \sum_{n=1}^{\infty}\frac{L}{n\pi}\frac{\mu^4}{n^4 - \mu^4}F_n\right), \tag{69}$$

$$V_2 = \left(\frac{3}{8}\frac{c}{L} + \sum_{n=1}^{\infty}\frac{L}{n\pi}\frac{(-1)^{n+1}\mu^4}{n^4 - \mu^4}F_n\right). \tag{70}$$

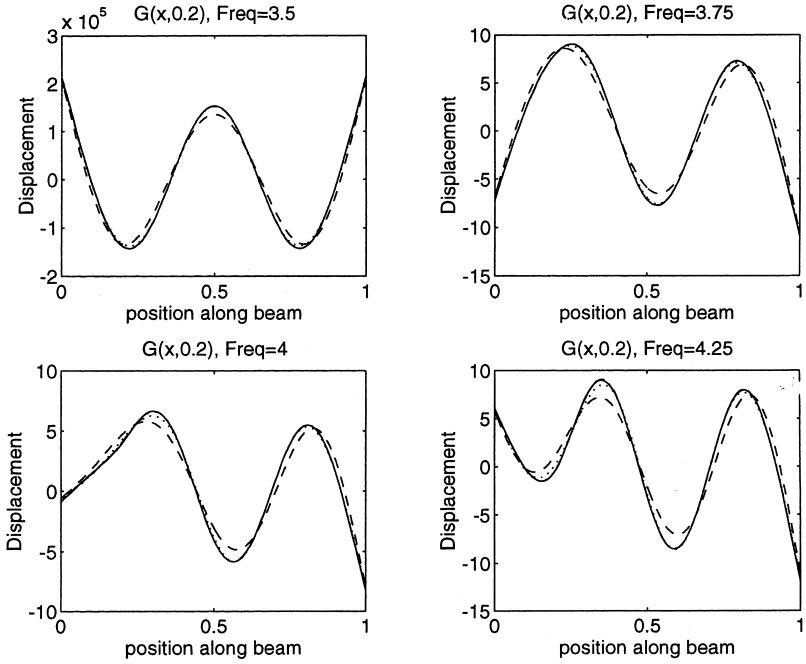

Fig. 1. Convergence of the Green function for the beam with number of terms in the series: (– – –) $N=4$; (· · ·)$N=6$; (–·–·–) $N=8$; (—) closed form solution.

It may be noted that

$$\lim_{c\to 0} F_n = \frac{3}{L\gamma_n}\left[1 - 2\left(1 - \frac{\gamma_n^2}{6} + \cdots\right) + 2\left(\frac{1}{2} - \frac{\gamma_n^2}{24} + \cdots\right)\right] = \mathrm{O}(c)$$

and therefore the standard tip receptances are again retrieved.

6. Numerical results for the beam

In the following, we plot the dimensionless quantities $(\pi^3 EI/L^3)g(x;x')$ and $(\pi^3 EI/L^3)v_d(x)$ against non-dimensional distance along the beam, x/l. The choice of x' is not important in the assessment of accuracy, and we have used $x' = 0.2l$ and $0.25l$ in the following. First, we compare the closed form expression and series form A for the Green function over a range of frequencies. The natural frequencies of the simply supported beam correspond to μ taking integer values, m say, and those of the free–free beam correspond very closely to $(m + 1/2)$ (the sequence is 1.50562, 2.49975, 3.50001, …). Fig. 1a–d shows results for $x' = 0.2l$ and $\mu - \epsilon = 3.50$, 3.75, 4.00 and 4.25, where ϵ is taken as 10^{-6} to avoid the precise singularities at the frequencies of the simply supported beam. In each of these figures the result from the closed form expression, Eq. (13), is shown with the continuous lines; the discontinous lines show the convergence of the series form with 4, 6 and 8 terms, respectively. The convergence of the series form to the closed form result is seen to be satisfactory, both near the free–free beam third natural frequency (Fig. 1a); near the fourth simply supported beam natural frequency (Fig. 1c); and at points well separated from either of these frequencies. The very close proximity to the free–free beam resonance accounts for the very large values in Fig. 1a. It is clear that taking four terms in the series is insufficient in this range of frequencies, whereas 8 terms yield converged results to within plotting accuracy.

Next, we examine convergence at much higher frequencies. Fig. 2a–d shows results from the series solution at frequencies corresponding to $\mu - \epsilon = 9.50$, 9.75, 10.00 and 10.25 and for $x' = 0.25l$. These include behaviour very close to the ninth free–free beam natural frequency and the tenth natural frequency of the simply-supported beam. The four lines in each figure correspond to results from 8, 12, 16 and 20 terms in the series. Convergence seems to be satisfactory. A rough rule of thumb would appear to be that one should use twice as many terms as the index n defining the nearest simply supported beam resonant frequency (in this case 10), to obtain results within plotting accuracy.

These results have used series form A for the Green function, which uses the Stokes transformation and closures of certain infinite series. We now examine results from the much simpler approach of series form B, based on the energy formulation leading to Eq. (58). Fig. 3 shows the Green functions using the different methods, at a frequency corresponding to $\mu = 7.75$. Fig. 3a and b are for $x' = 0$, while Fig. 3c and d are for $x'/L = 0.25$. Each figure shows three curves: the solid line is obtained from the exact

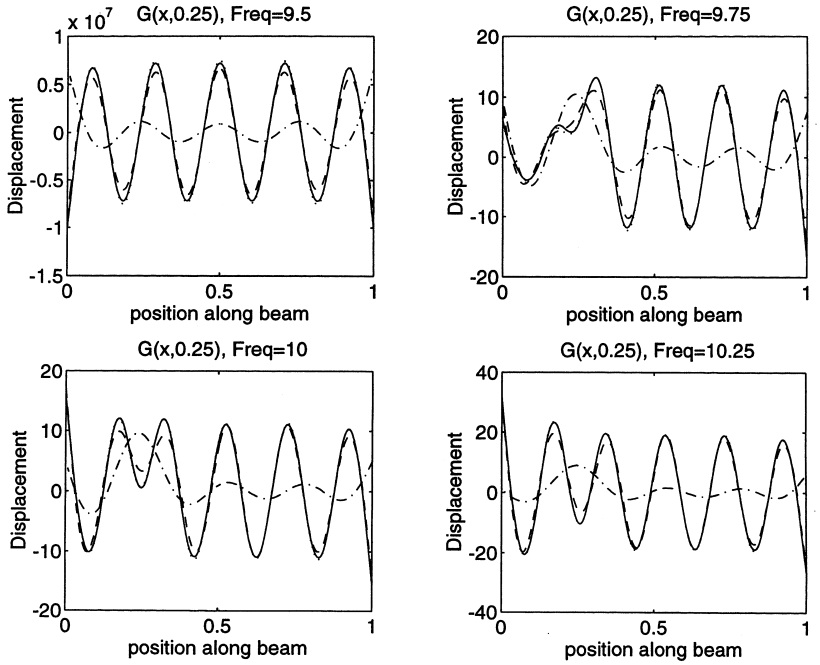

Fig. 2. Convergence of the Green function for the beam with number of terms in the series: (– – –) $N = 8$; (· · ·)$N = 12$; (–·–·–)$N = 16$; (—) $N = 20$.

solution, Eq. (13); the dashed–dotted line is from series form A; and the dashed line is from series form B. Fig. 3a and c uses 8 terms in the series solutions, and 12 terms are used for the results in Fig. 3b and d. One observes from these and other similar results that series form A converges slightly faster than form B, but both converge satisfactorily to within plotting accuracy for a number of terms equal to twice the mode number of the nearest natural frequency (mode 7 in this case). We also note that there is no particular difficulty in obtaining convergence with either method even

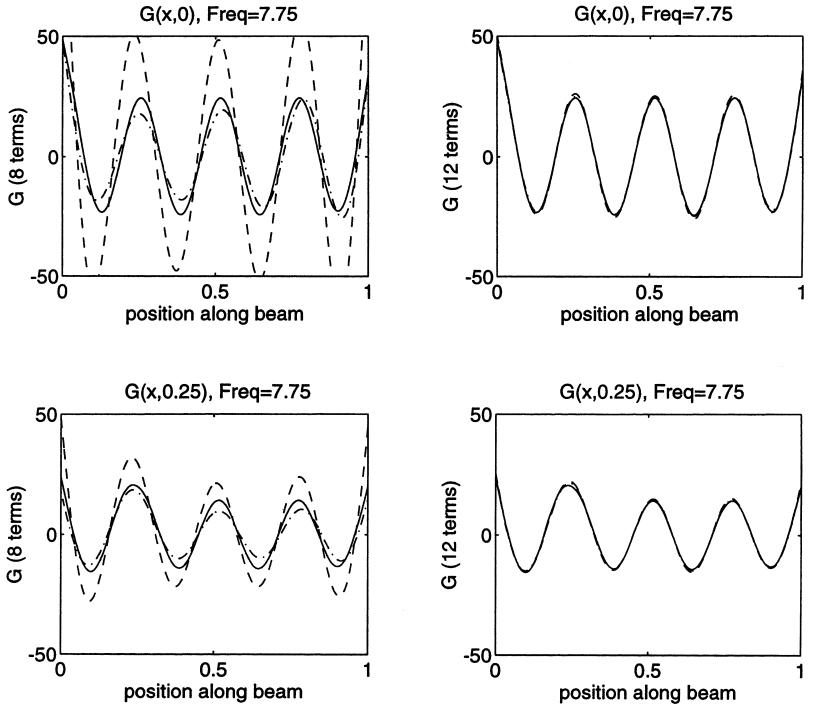

Fig. 3. Green functions for the beam: (—) closed form solution; (–·–·–) series form A; (– – –) series form B. $G(x, 0)$ for: (a) 8 terms and (b) 12 terms in the series; $G(x, 0.25)$ for: (c) 8 terms and (d) 12 terms in the series.

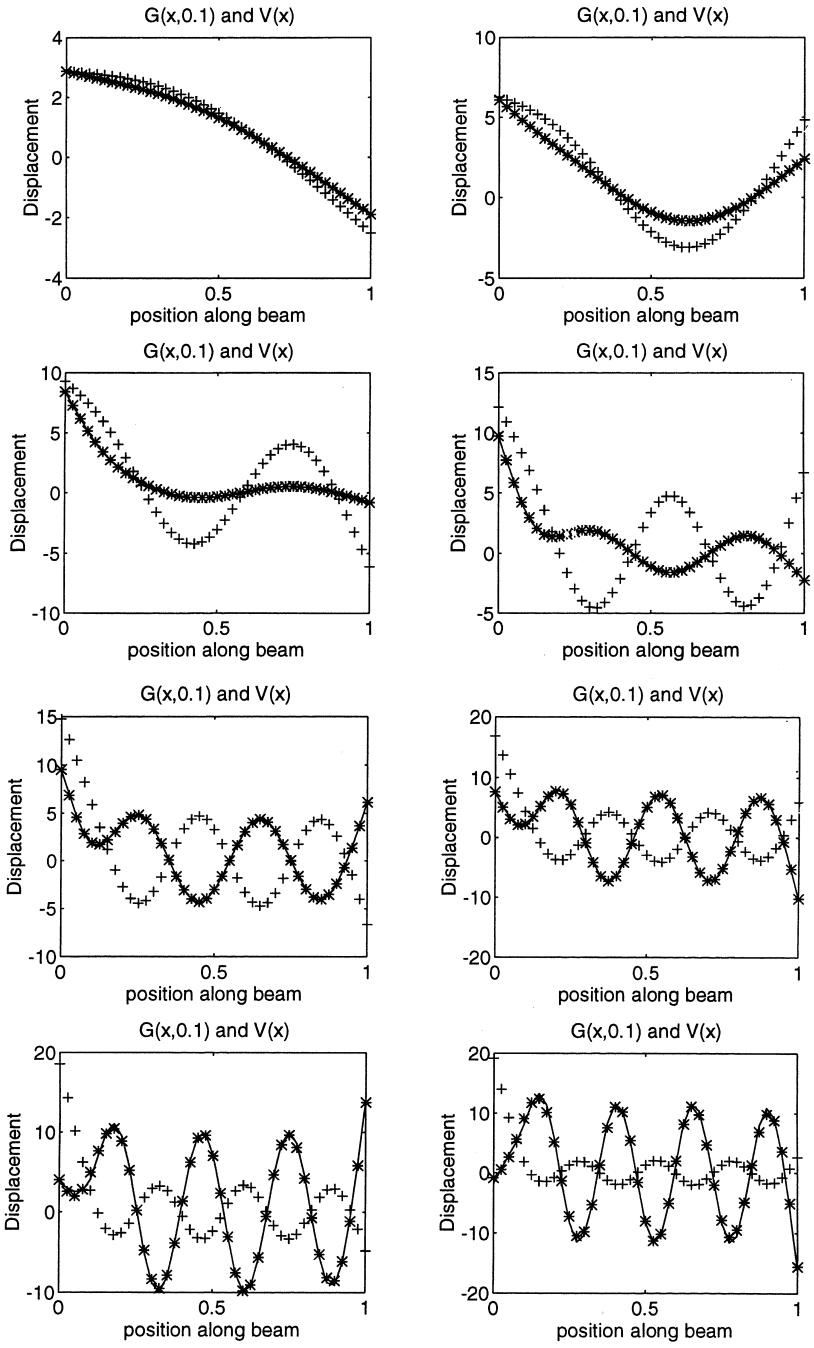

Fig. 4. The Green function ($*\ *\ *\ *$) and the displacement due to a parabolically varying load ($+++$) over a length $c = 0.1\,L$ of the beam: (a) $\mu = 1$; (b) $\mu = 2$; (c) $\mu = 3$; (d) $\mu = 4$; (e) $\mu = 5$; (f) $\mu = 6$; (g) $\mu = 7$; (h) $\mu = 8$.

when the point load is at the end of the beam. Additional results confirm that the natural frequencies and mode shapes of the free–free beam converge equally satisfactorily.

Finally, we illustrate the analysis for a distributed load such as discussed in Section 5. Figs. 4–8 give results for the five cases $c/L = 0.1$, 0.3, 0.5, 0.7 and 0.9. For each case, results are given at 8 frequencies, corresponding to $\mu - \epsilon = 1, 2, \ldots 8$. Each figure shows the displacement $V(x)$ under the corresponding distributed load (plotted with the '+') and the Green function for a point load at $x'/L = 0.1$. The Green function is calculated from the closed form expression (the solid line), and the series A solution with 20 terms (plotted with the '$*$'). It may be seen that, as expected, at low frequencies the results for the parabolic load distributed over the length $c/L = 0.3$ are very close to the Green function for a load at $x'/L = 0.1$. At

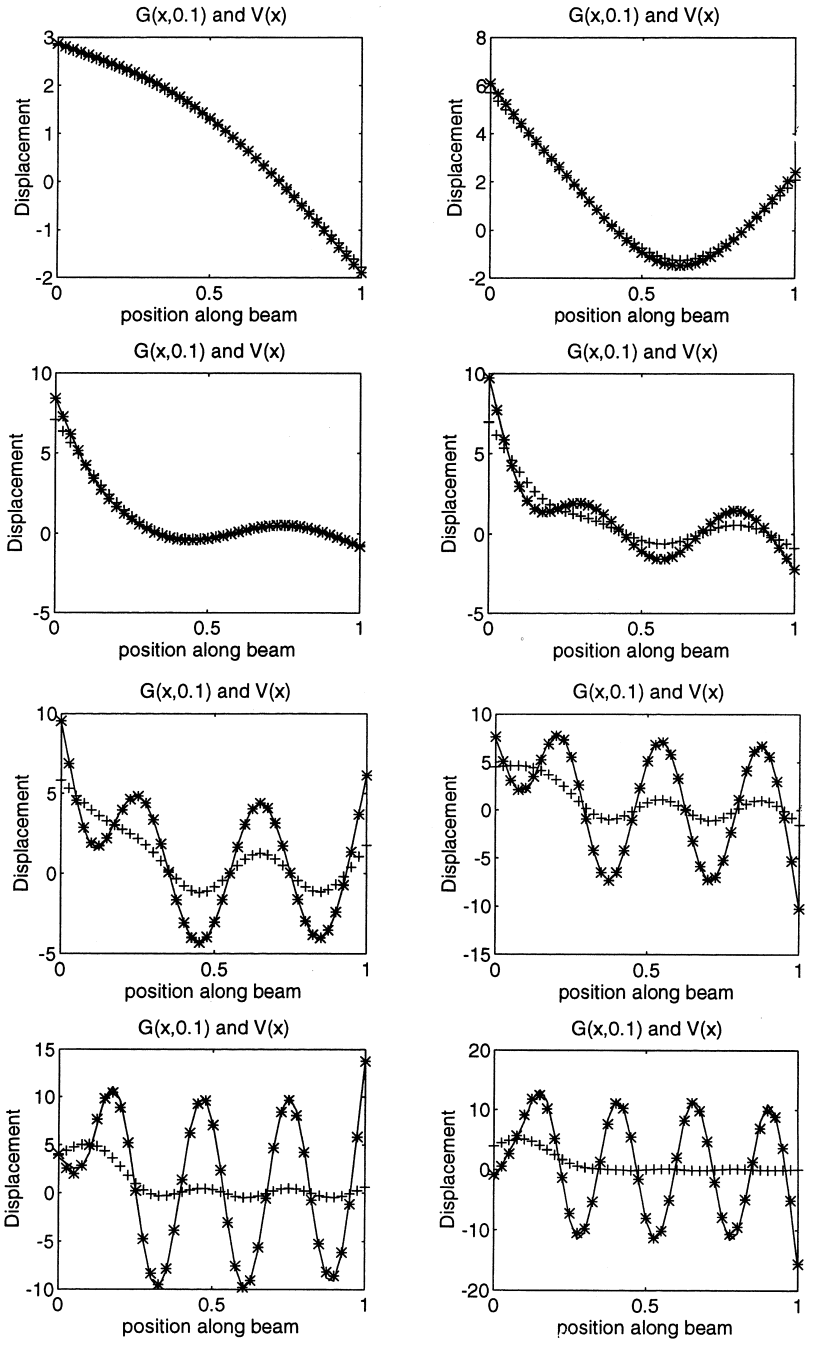

Fig. 5. The Green function (* * * *) and the displacement due to a parabolically varying load (++++) over a length $c = 0.3\,L$ of the beam: (a) $\mu = 1$; (b) $\mu = 2$; (c) $\mu = 3$; (d) $\mu = 4$; (e) $\mu = 5$; (f) $\mu = 6$; (g) $\mu = 7$; (h) $\mu = 8$.

higher frequencies, however, the effect of distributing the load is to increase the participation of many more modes (since these results are not at the resonances of the free–free beam). This has an averaging effect, which reduces the degree of oscillation along the beam. If, however, the vibration frequency corresponds to a resonance of the free–free beam, of course the response to the distributed load and the Green function both match the corresponding mode shape. (cf. Figs. 1a and 2a for the third and ninth modes, respectively).

7. Derivation of the green function for the plate

We now develop the Green function for a free-free plate, basing the procedure on the energy method analogous to the

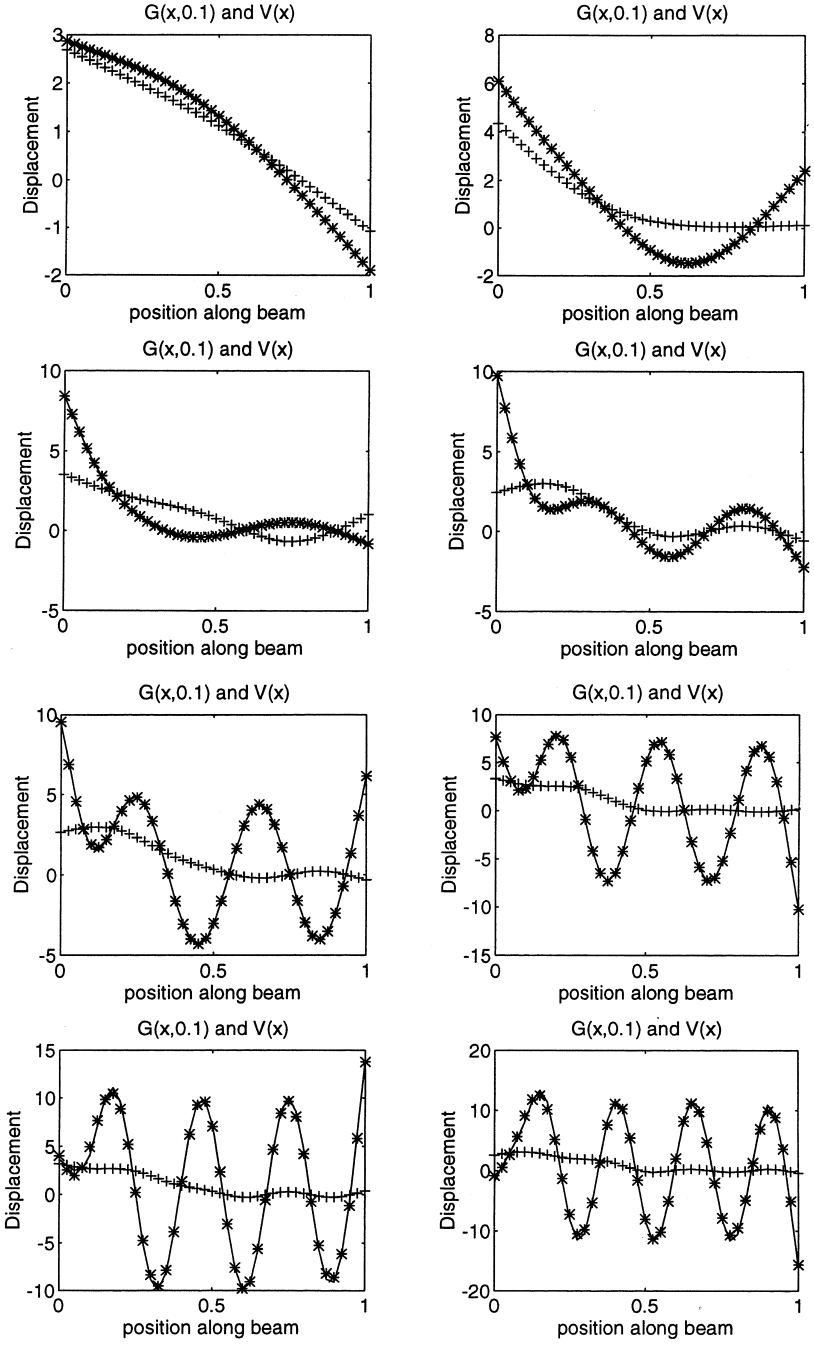

Fig. 6. The Green function ($*\ *\ *\ *$) and the displacement due to a parabolically varying load ($+++$) over a length $c = 0.5\,L$ of the beam: (a) $\mu = 1$; (b) $\mu = 2$; (c) $\mu = 3$; (d) $\mu = 4$; (e) $\mu = 5$; (f) $\mu = 6$; (g) $\mu = 7$; (h) $\mu = 8$.

derivation of the series form B in the case of the beam. (It does not appear at all straightforward to obtain for the plate the equivalent of series form A).

We define axes *OXY* directed along two adjacent edges of the plate, and define the transverse deflection as $w(X,Y)$ — as in Section 4.3, we have factored out the time dependence for harmonic response. The length and breadth of the plate are a and b, respectively, and we define the aspect ratio by $r = b/a$. It is convenient to use non-dimensional coordinates $x = X/a$ and $y = Y/b$. Assuming that the plate is thin so that shear deformations are negligible, we use the standard strain energy expression:

$$U = \frac{D}{2ab}\int_0^1\int_0^1\left[r^2\left(\frac{\partial^2 w}{\partial x^2}\right)^2 + \frac{1}{r^2}\left(\frac{\partial^2 w}{\partial y^2}\right)^2 + 2\nu\frac{\partial^2 w}{\partial x^2}\frac{\partial^2 w}{\partial y^2} + 2(1-\nu)\left(\frac{\partial^2 w}{\partial x \partial y}\right)^2\right]\mathrm{d}x\,\mathrm{d}y, \tag{71}$$

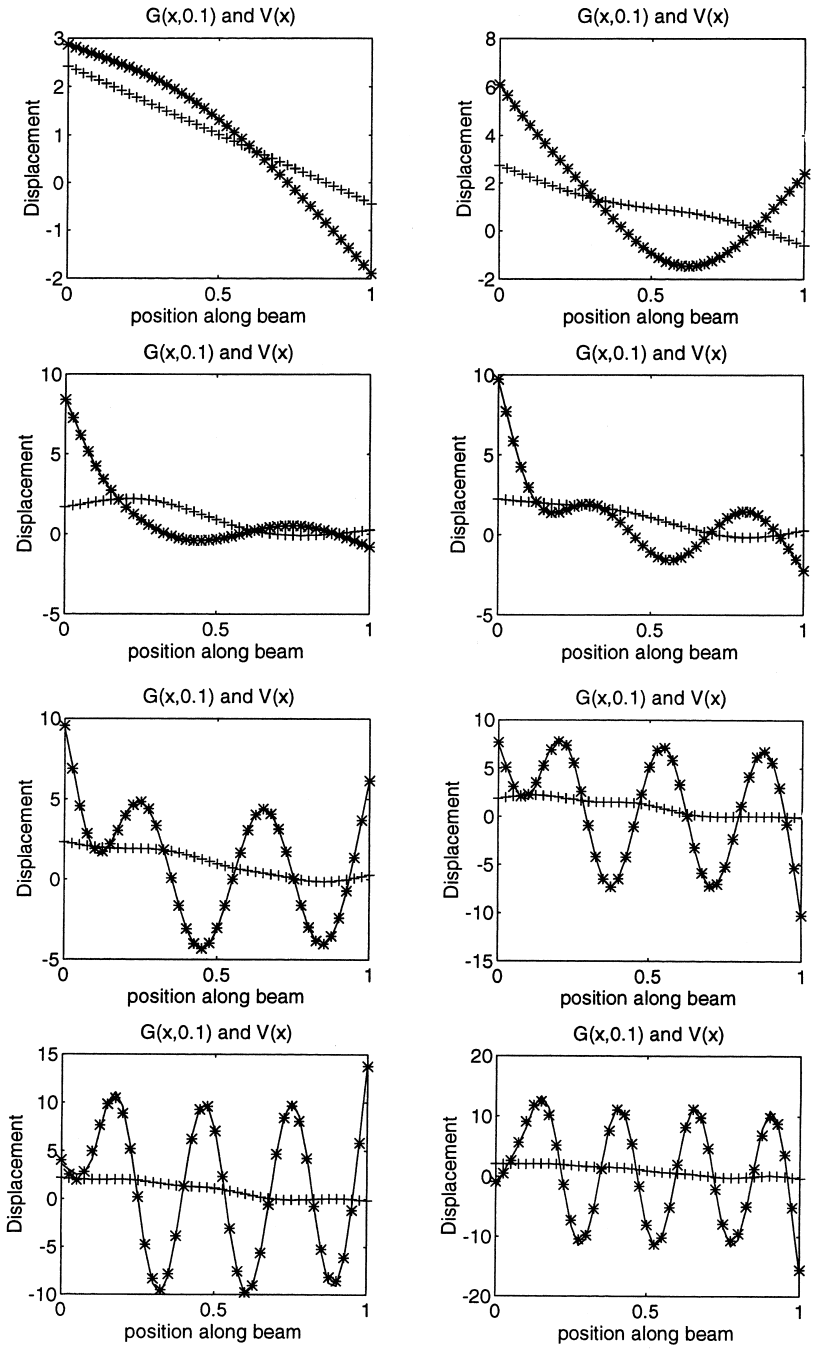

Fig. 7. The Green function (* * * *) and the displacement due to a parabolically varying load (++++) over a length $c = 0.7\,L$ of the beam: (a) $\mu = 1$; (b) $\mu = 2$; (c) $\mu = 3$; (d) $\mu = 4$; (e) $\mu = 5$; (f) $\mu = 6$; (g) $\mu = 7$; (h) $\mu = 8$.

where D is the flexural rigidity and ν is Poisson's ratio. The kinetic energy, ignoring rotary inertia, is:

$$T = \frac{1}{2}\omega^2 \gamma ab \int_0^1 \int_0^1 w^2 \, \mathrm{d}x \, \mathrm{d}y, \tag{72}$$

where γ is the mass per unit area. The potential of an applied load $f(x,y)$ is:

$$V = -ab \int_0^1 \int_0^1 fw \, \mathrm{d}x \, \mathrm{d}y, \tag{73}$$

where to obtain the Green function we take

$$f(x,y) = \delta(x - x')\delta(y - y'). \tag{74}$$

For the deflected shape of the plate, we use an analogous

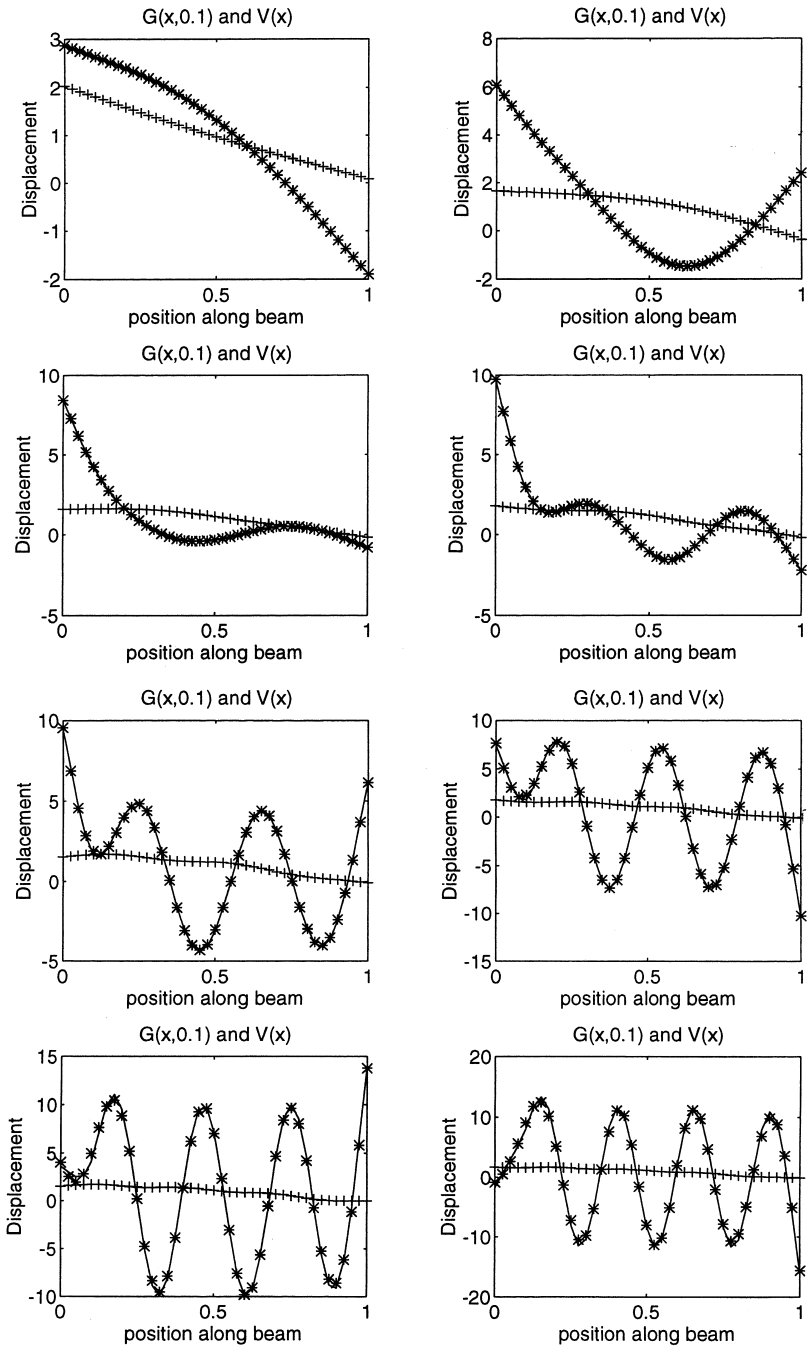

Fig. 8. The Green function (* * * *) and the displacement due to a parabolically varying load (+ + + +) over a length $c = 0.9\,L$ of the beam: (a) $\mu = 1$; (b) $\mu = 2$; (c) $\mu = 3$; (d) $\mu = 4$; (e) $\mu = 5$; (f) $\mu = 6$; (g) $\mu = 7$; (h) $\mu = 8$.

expression to the simple formulation in Eq. (14) for the beam, i.e.

$$w = c_0 + c_1 x + c_2 y + c_3 xy + \sum_m [u_{0m}(1-y) + u_{1m} y] \sin m\pi x + \sum_m [v_{0m}(1-x) + v_{1m} x] \sin m\pi y + \sum_m \sum_n P_{mn} \sin m\pi x \sin n\pi y. \quad (75)$$

This contains the rigid body modes explicitly, sinusoidal modes in each direction, and cross terms. In obtaining numerical results, the series will be truncated appropriately.

Performing the integrations, and applying the variational principle as stated in Eq. (53), we again obtain Eq. (58) where now the matrices take the following forms:

$$\mathbf{Q}^{\mathrm{T}} = [\,\mathbf{Q_c} \quad \mathbf{Q_{u0}} \quad \mathbf{Q_{u1}} \quad \mathbf{Q_{v0}} \quad \mathbf{Q_{v1}} \quad \mathbf{Q_P}\,], \quad (76)$$

where

$$\mathbf{Q_c} = [\,c_0 \quad c_1 \quad c_2 \quad c_3\,], \qquad \mathbf{Q_{u0}} = [\,u_{01} \quad u_{02} \quad \ldots\,], \tag{77}$$

$$\mathbf{Q_{u1}} = [\,u_{11} \quad u_{12} \quad \ldots\,], \qquad \mathbf{Q_{v0}} = [\,v_{01} \quad v_{02} \quad \ldots\,],$$

$$\mathbf{Q_{v1}} = [\,v_{11} \quad v_{12} \quad \ldots\,],$$

$$\mathbf{Q_P} = [\,P_{11} \quad P_{12} \quad \ldots \quad P_{21} \quad P_{22} \quad \ldots\,];$$

$$\mathbf{F}(x'y')^{\mathrm{T}} = [\,\mathbf{F_c} \quad \mathbf{F_{u0}} \quad \mathbf{F_{u1}} \quad \mathbf{F_{v0}} \quad \mathbf{F_{v1}} \quad \mathbf{F_P}\,], \tag{78}$$

where

$$\mathbf{F_c} = [1\ x'\ y'\ x'y'],$$

$$\mathbf{F_{u0}} = (1-y')[\sin\pi x'\ \sin 2\pi x' \ldots],$$

$$\mathbf{F_{u1}} = y'[\sin\pi x'\ \sin 2\pi x' \ldots],$$

$$\mathbf{F_{v0}} = (1-x')[\sin\pi y'\ \sin 2\pi y' \ldots],$$

$$\mathbf{F_{v1}} = x'[\sin\pi y'\ \sin 2\pi y' \ldots],$$

$$\mathbf{F_P} = [\sin\pi x'\ \sin\pi y' \quad \sin\pi x'\ \sin 2\pi y' \ldots$$
$$\sin 2\pi x'\ \sin\pi y' \quad \sin 2\pi x'\ \sin 2\pi y' \ldots];$$

$$\mathbf{K} = \frac{D}{ab}\begin{bmatrix} \mathbf{K}_{cc} & \mathbf{0} & \mathbf{0} & \mathbf{0} & \mathbf{0} & \mathbf{0} \\ \mathbf{0} & \mathbf{K}_{u0u0} & \mathbf{K}_{u0u1} & \mathbf{K}_{u0v0} & \mathbf{K}_{u0v1} & \mathbf{K}_{u0P} \\ \mathbf{0} & \mathbf{K}^{\mathrm{T}}_{u0u1} & \mathbf{K}_{u1u1} & \mathbf{K}_{u1v0} & \mathbf{K}_{u1v1} & \mathbf{K}_{u1P} \\ \mathbf{0} & \mathbf{K}^{\mathrm{T}}_{u0v0} & \mathbf{K}^{\mathrm{T}}_{u1v0} & \mathbf{K}_{v0v0} & \mathbf{K}_{v0v1} & \mathbf{K}_{v0P} \\ \mathbf{0} & \mathbf{K}^{\mathrm{T}}_{u0v1} & \mathbf{K}^{\mathrm{T}}_{u1v1} & \mathbf{K}^{\mathrm{T}}_{v0v1} & \mathbf{K}_{v1v1} & \mathbf{K}_{v1P} \\ \mathbf{0} & \mathbf{K}^{\mathrm{T}}_{u0P} & \mathbf{K}^{\mathrm{T}}_{u1P} & \mathbf{K}^{\mathrm{T}}_{v0P} & \mathbf{K}^{\mathrm{T}}_{v1P} & \mathbf{K}_{PP} \end{bmatrix}; \tag{79}$$

and

$$\mathbf{M} = \gamma ab\begin{bmatrix} \mathbf{M}_{cc} & \mathbf{M}_{cu0} & \mathbf{M}_{cu1} & \mathbf{M}_{cv0} & \mathbf{M}_{cv1} & \mathbf{M}_{cP} \\ \mathbf{M}^{\mathrm{T}}_{cu0} & \mathbf{M}_{u0u0} & \mathbf{M}_{u0u1} & \mathbf{M}_{u0v0} & \mathbf{M}_{u0v1} & \mathbf{M}_{u0P} \\ \mathbf{M}^{\mathrm{T}}_{cu1} & \mathbf{M}^{\mathrm{T}}_{u0u1} & \mathbf{M}_{u1u1} & \mathbf{M}_{u1v0} & \mathbf{M}_{u1v1} & \mathbf{M}_{u1P} \\ \mathbf{M}^{\mathrm{T}}_{cv0} & \mathbf{M}^{\mathrm{T}}_{u0v0} & \mathbf{M}^{\mathrm{T}}_{u1v0} & \mathbf{M}_{v0v0} & \mathbf{M}_{v0v1} & \mathbf{M}_{v0P} \\ \mathbf{M}^{\mathrm{T}}_{cv1} & \mathbf{M}^{\mathrm{T}}_{u0v1} & \mathbf{M}^{\mathrm{T}}_{u1v1} & \mathbf{M}^{\mathrm{T}}_{v0v1} & \mathbf{M}_{v1v1} & \mathbf{M}_{v1P} \\ \mathbf{M}^{\mathrm{T}}_{cP} & \mathbf{M}^{\mathrm{T}}_{u0P} & \mathbf{M}^{\mathrm{T}}_{u1P} & \mathbf{M}^{\mathrm{T}}_{v0P} & \mathbf{M}^{\mathrm{T}}_{v1P} & \mathbf{M}_{PP} \end{bmatrix}. \tag{80}$$

The submatrices are given by

$$\mathbf{K}_{cc} = \begin{bmatrix} 0 & 0 & 0 & 0 \\ 0 & 0 & 0 & 0 \\ 0 & 0 & 0 & 0 \\ 0 & 0 & 0 & 2(1-\nu) \end{bmatrix};$$

$$K_{u0mu0m'} = [\tfrac{1}{6}\pi^4 m^4 r^2 + (1-\nu)m^2\pi^2]\delta_{mm'};$$

$$K_{u0mu1m'} = [\tfrac{1}{12}\pi^4 m^4 r^2 - (1-\nu)m^2\pi^2]\delta_{mm'};$$

$$K_{u1mu1m'} = [\tfrac{1}{6}\pi^4 m^4 r^2 + (1-\nu)m^2\pi^2]\delta_{mm'};$$

$$K_{u0mv0n} = \nu\pi^2 mn; \qquad K_{u1mv0n} = \nu\pi^2 mn\epsilon_n;$$

$$K_{u0mv1n} = \nu\pi^2 mn\epsilon_m; \qquad K_{u1mv1n} = \nu\pi^2 mn\epsilon_{m+n};$$

$$K_{v0nv0n'} = [\tfrac{1}{6}\pi^4\frac{n^4}{r^2} + (1-\nu)n^2\pi^2]\delta_{nn'};$$

$$K_{v0nv1n'} = [\tfrac{1}{12}\pi^4\frac{n^4}{r^2} - (1-\nu)n^2\pi^2]\delta_{nn'};$$

$$K_{v1nv1n'} = [\tfrac{1}{6}\pi^4\frac{n^4}{r^2} + (1-\nu)n^2\pi^2]\delta_{nn'};$$

$$K_{u0m'Pmn} = \frac{m^2\pi^3}{2}\left(\frac{m^2r^2}{n} + \nu n\right);$$

$$K_{u1m'Pmn} = \frac{m^2\pi^3}{2}\left(\frac{m^2r^2}{n} + \nu n\right)\epsilon_n;$$

$$K_{v0n'Pmn} = \frac{n^2\pi^3}{2}\left(\frac{n^2}{r^2m} + \nu m\right);$$

$$K_{v1n'Pmn} = \frac{n^2\pi^3}{2}\left(\frac{n^2}{r^2m} + \nu m\right)\epsilon_m;$$

$$K_{Pm'n'Pmn} = \frac{\pi}{4}\left(rm^2 + \frac{n^2}{r}\right)^2\delta_{mm'}\delta_{nn'};$$

$$\mathbf{M}_{cc} = \begin{bmatrix} 1 & \frac{1}{2} & \frac{1}{2} & \frac{1}{4} \\ \frac{1}{2} & \frac{1}{3} & \frac{1}{4} & \frac{1}{6} \\ \frac{1}{2} & \frac{1}{4} & \frac{1}{3} & \frac{1}{6} \\ \frac{1}{4} & \frac{1}{6} & \frac{1}{6} & \frac{1}{9} \end{bmatrix};$$

$$M_{c0u0m} = \frac{1+\epsilon_m}{2m\pi} = M_{c0u1m};$$

$$M_{c0v0n} = \frac{1+\epsilon_n}{2n\pi} = M_{c0v1m};$$

$$M_{c1u0m} = \frac{\epsilon_m}{2m\pi} = M_{c1u1m};$$

$$M_{c1v0n} = \frac{1+\epsilon_n}{6n\pi};$$

$$M_{c1v1n} = \frac{1+\epsilon_n}{3n\pi};$$

Table 1
Non-dimensional natural frequencies, σ_i, versus number of Fourier harmonics in each direction, N, for a square free–free plate

N	σ_4	σ_5	σ_6	σ_7	σ_8	σ_9	σ_{10}	σ_{11}	σ_{12}	σ_{13}
2	13.20	19.38	25.51	35.17	35.17	63.36	63.36	68.68	69.15	81.97
4	13.18	19.33	24.63	34.42	34.42	61.43	61.43	63.10	68.58	77.85
8	13.18	19.29	24.50	34.34	34.34	61.15	61.15	62.92	68.48	77.30
16	13.17	19.26	24.46	34.29	34.29	61.04	61.04	62.85	68.35	77.13
32	13.17	19.24	24.44	34.26	34.26	60.99	60.99	62.81	68.25	77.05

$$M_{c2u0n} = \frac{1+\epsilon_m}{6m\pi};$$

$$M_{c2u1n} = \frac{1+\epsilon_m}{3n\pi};$$

$$M_{c2v0n} = \frac{\epsilon_n}{2n\pi} = M_{c2v1n};$$

$$M_{c3u0m} = \frac{\epsilon_m}{6m\pi};$$

$$M_{c3u1m} = \frac{\epsilon_m}{3m\pi};$$

$$M_{c3v0n} = \frac{\epsilon_n}{6n\pi};$$

$$M_{c3v1n} = \frac{\epsilon_n}{3n\pi};$$

$$M_{c0Pmn} = \frac{(1+\epsilon_m)(1+\epsilon_n)}{mn\pi^2};$$

$$M_{c1Pmn} = \frac{\epsilon_m(1+\epsilon_n)}{mn\pi^2};$$

$$M_{c2Pmn} = \frac{(1+\epsilon_m)\epsilon_n}{mn\pi^2};$$

$$M_{c3Pmn} = \frac{\epsilon_m\epsilon_n}{mn\pi^2};$$

$$M_{u0mu0m'} = \tfrac{1}{6}\delta_{mm'} = M_{u1mu1m'};$$

$$M_{u0mu1m'} = \tfrac{1}{12}\delta_{mm'};$$

$$M_{u0mv0n} = \frac{1}{mn\pi^2}; \qquad M_{u0mv1n} = \frac{\epsilon_m}{mn\pi^2};$$

$$M_{u1mv0n} = \frac{\epsilon_n}{mn\pi^2}; \qquad M_{u1mv1n} = \frac{\epsilon_{m+n}}{mn\pi^2};$$

$$M_{v0nv0n'} = \tfrac{1}{6}\delta_{nn'} = M_{v1nv1n'};$$

$$M_{v0nv1n'} = \tfrac{1}{12}\delta_{nn'};$$

$$M_{u0m'Pmn} = \frac{1}{2n\pi}\delta_{mm'}; \qquad M_{u1m'Pmn} = \frac{\epsilon_n}{2n\pi}\delta_{mm'};$$

$$M_{v0n'Pmn} = \frac{1}{2m\pi}\delta_{nn'}; \qquad M_{v1n'Pmn} = \frac{\epsilon_m}{2m\pi}\delta_{nn'};$$

$$M_{PmnPm'n'} = \tfrac{1}{4}\delta_{mm'}\delta_{nn'};$$

where $\delta_{mm'}$ is the Kronecker delta, and

$$\epsilon_m = -(-1)^m.$$

Based on these definitions for **K**, **M** and **F**, we may then solve Eq. (58) for **Q**, truncating at finite values of m and n corresponding to the sinusoidal terms in the x and y directions. Hence, we obtain the plate Green function as

$$g(x,y;x',y') = \mathbf{F}^{\mathrm{T}}(x,y)[\mathbf{K} - \mu^4\mathbf{M}]^{-1}\mathbf{F}(x',y'). \tag{81}$$

We may also solve the generalised eigenvalue problem

$$[\mathbf{K} - \mu^4\mathbf{M}]\mathbf{Q} = 0 \tag{82}$$

to obtain the natural frequencies and mode shapes for the plate.

8. Numerical results for the plate

We consider first the natural frequencies and mode shapes of the free–free plate, based on the above formulation. We take $\nu = 0.333$ for all of the results shown here. Table 1 shows predictions of the first ten non-zero natural frequencies for a square plate, using 2, 4, 8, 16 and 32 harmonics in the Fourier series in each direction. Thus with eight terms, for example, there are 100 unknowns in the vector **Q**. The frequencies are expressed in non-dimensional form as $\sigma_i = \omega_i b^2\sqrt{\gamma/\mathrm{D}}$, where $i = 1, 2, 3$ correspond to the first three

Table 2
Non-dimensional natural frequencies, σ_i, versus number of Fourier harmonics in each direction, N, for a free–free plate ($b/a = 5$)

N	σ_4	σ_5	σ_6	σ_7	σ_8	σ_9	σ_{10}	σ_{11}	σ_{12}	σ_{13}
2	21.68	60.58	63.63	145.45	227.0	566.9	583.2	643.5	735.9	1576.2
4	21.30	59.12	63.46	119.3	131.0	198.6	205.2	315.8	415.3	559.8
8	21.22	58.85	63.43	116.1	130.3	193.0	203.8	287.0	290.4	381.8
16	21.19	58.75	63.43	115.9	130.2	192.6	203.6	286.2	288.8	380.6
32	21.17	58.70	63.42	115.8	130.2	192.4	203.5	286.1	288.5	380.3

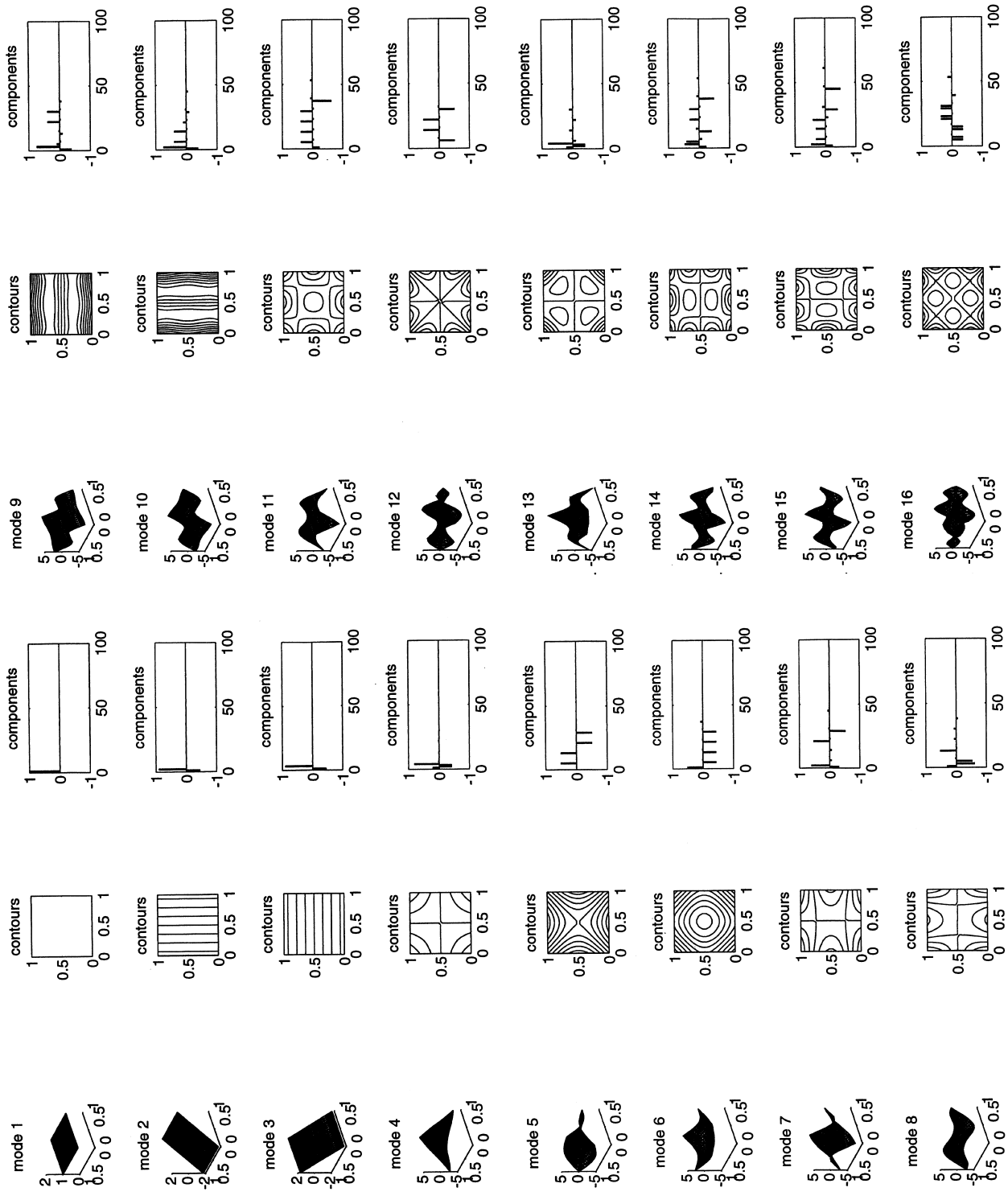

Fig. 9. Mode shapes and natural frequencies for free-free plate (square), based on eight Fourier harmonics ($\sigma_i = \omega_i b^2 \sqrt{\gamma/D}$).

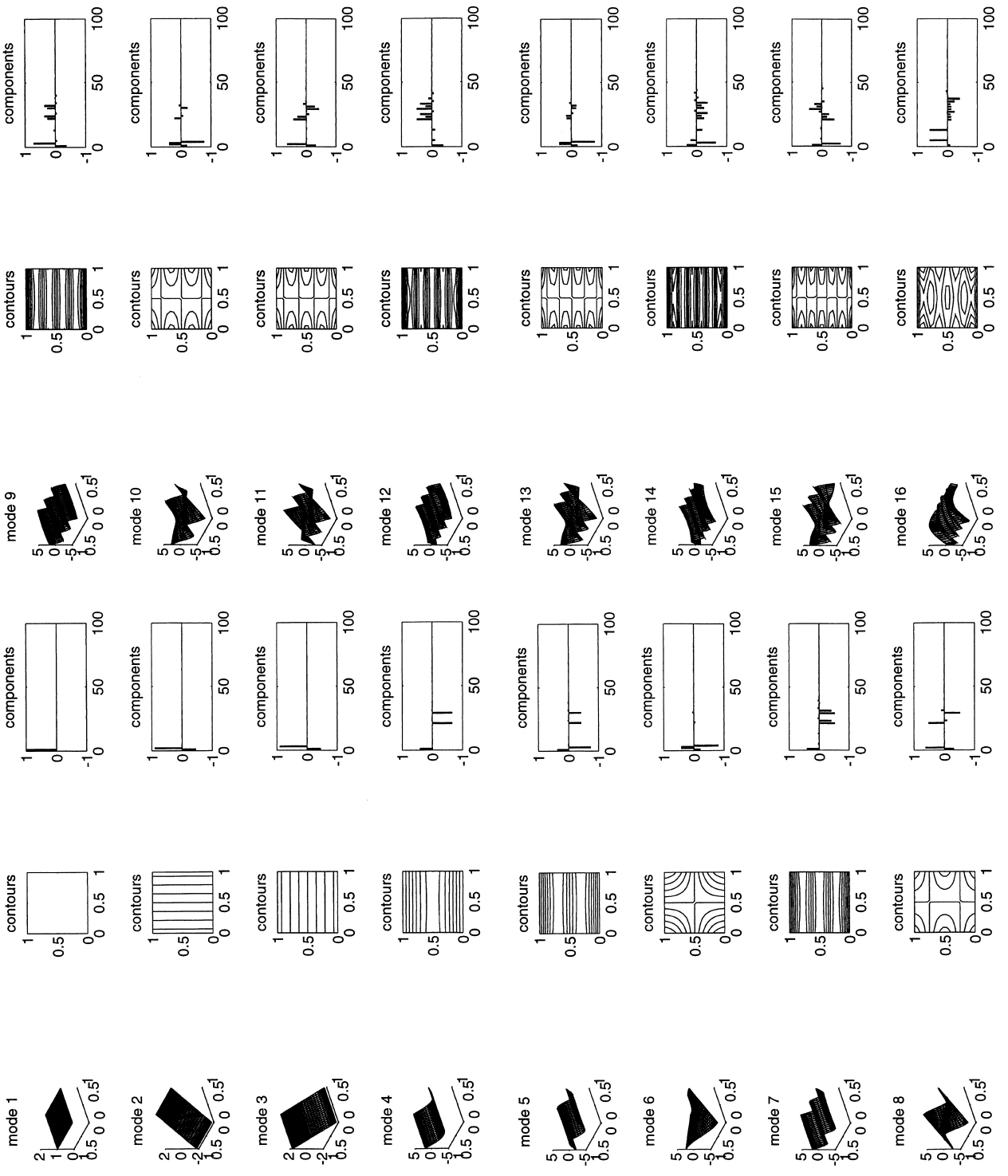

Fig. 10. Mode shapes and natural frequencies for free-free plate ($a/b = 5$), based on eight Fourier harmonics.

rigid body modes. Table 2 shows equivalent results for a rectangular plate with $b/a = 5$. In both cases, the convergence is seen to be satisfactory. The results for the square plate computed with 32 harmonics in each direction are within about 0.1% of those tabulated by Gorman and Wei Din [15], based on a superposition approach for the thin plate problem. The first 16 modes in each case are shown in Figs. 9 and 10, respectively, including the rigid body modes. These results are based on using eight terms in each direction, though the results based on 32 terms are almost indistinguishable. Also shown in these figures are all the components of the vector **Q** for each mode plotted (which has 100 elements for the representation with 8 harmonics in each direction: 4 for c_i, 32 for the terms in u and v, and 64 for the P_{mn}). It should be noted that the isometrics and contour plots in Fig. 10 are shown on a square, because the spatial dimensions have been non-dimensionalised by the sides of the plate. The beam-type behaviour for $b/a = 5$ is, however, clearly apparent in modes 4, 5, 7, 9, 12 and 14. On the other hand, when scaled to the square, modes 6 and 8 of the rectangular plate clearly correspond to modes 4 and 7 for the square plate. This may also be observed in the components of **Q**. Furthermore, it is seen that for the first 16 modes, in either case, the terms P_{mn} do not contribute greatly (though their effect is not negligible).

A sample of Green functions for the free–free square plate is shown in Fig. 11, for a non-dimensional frequency $\sigma = 20.00$. The nine plots show the values of the Green function $G(x',y') = g(x,y,x',y')$ corresponding to nine positions (x',y') of a point load in one quadrant of the plate. It may be seen that, as expected, mode 5 is excited ($\sigma_5 = 19.24$ from Table 1), except when the load is on the diagonal of the square which is a nodal line for this mode.

9. Discussion

This analysis has led first to a form of Green function for the free–free beam which is based on a sum of modes for a simply supported beam plus the two rigid body modes. The two approaches adopted (selection of a series to satisfy the conditions of the boundary values problem directly, and use of an energy formulation which satisfies the natural boundary conditions implicitly) have both been shown to be very satisfactory. Numerical results suggest that the series converge rapidly. For example, at frequencies in the region of the nth resonant frequency of the simply supported beam, about $2n$ terms are required in the series to obtain the Green function for the free–free beam. The series form may be used without difficulty at very high frequencies, without the special treatment required in the case of the closed form expression corresponding to the free–free beam.

The second approach has then been used for the thin plate. Natural frequencies and mode shapes for square and rectangular free–free plates have been evaluated, and it has been found that with 8 sinusoidal terms in each direction the first 13 modal frequencies are within 0.5% of the converged results. Green functions for the plate have also been obtained, which also appear to have satisfactory convergence characteristics.

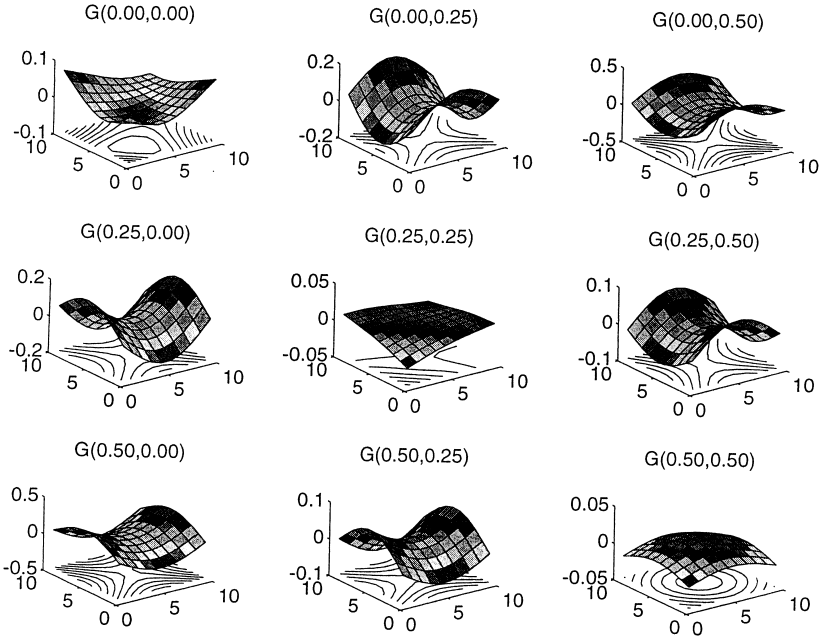

Fig. 11. Green functions for free–free plate (square) at $\sigma = 20.00$.

Acknowledgements

Part of this work was completed during a visit by the first author to the Research Institute for Applied Mechanics. He is very grateful for the support provided by the Institute and the Royal Society.

References

[1] Utsunomiya T, Watanabe T, Wu C, Hayashi N, Nakai K, Sekita K. Wave response analysis of a flexible floating structure by BE–FE combination method. In: Proceedings of Fifth International Offshore and Polar Engineering Conference. The Hague, The Netherlands, 1995. p. 400–5.

[2] Kashiwagi M. A B-spline Galerkin method for computing hydroelastic behaviour of a very large floating structure. Paper 36. In: Proceedings of International Workshop on Very Large Floating Structures. Hayama, Japan, 1996.

[3] Ohkusu M, Namba M. Hydroelastic response of a floating thin plate in very short waves. In: Proceedings of 12th International Workshop on Water Waves and Floating Bodies. Carry-le-Rouet, France, 1997. p. 207–10.

[4] Kagemoto H, Fujino M, Zhu T. On the estimation method of hydrodynamic forces acting on a very large floating structure. Applied Ocean Research 1997;19:49–60.

[5] Ohkusu M, Namba M. Hydroelastic behaviour of a very large floating platform in waves. In: Proceedings of 11th International Workshop on Water Waves and Floating Bodies. Hamburg, Germany, 1996.

[6] Hermans AJ. The excitation of waves in a very large floating flexible platform by short free surface waves. In: Proceedings of 12th International Workshop on Water Waves and Floating Bodies. Carry-le-Rouet, France, 1997. p. 107–10.

[7] Chen JT, Tsaur DH, Hong H-K. An alternative method for transient and random responses of structures subject to support motions. Engineering Structures 1997;19:162–72.

[8] Namba M, Ohkusu M. Hydroelastic behaviour of floating artificial islands in waves. International Journal of Offshore and Polar Engineering 1999:9.

[9] Leissa AW. The free vibration of rectangular plates. Journal of Sound and Vibration 1973;31:257–93.

[10] Bardell NS. Free vibration of a flat plate using the hierarchical finite element method. Journal of Sound and Vibration 1991;151:263–89.

[11] Beslin O, Nicolas J. A hierarchical function set for predicting very high order plate bending modes with any boundary conditions. Journal of Sound and Vibration 1997;202:633–55.

[12] Milne HK. On the receptance functions of a uniform beam. Journal of Sound and Vibration 1991;146:176–80.

[13] Beshara M. Energy flows in structures with compliant non-conservative couplings. Thesis submitted for DPhil, University of Oxford, 1997.

[14] Bromwich TJI. An introduction to the theory of infinite series. London: MacMillan, 1926.

[15] Gorman DJ, Ding Wei. Accurate free vibration analysis of the completely free rectangular Mindlin plate. Journal of Sound and Vibration 1996;189:341–53.